Optical investigation of semi-polar (11-22) $Al_xGa_{1-x}N$ with high Al composition

Z. Li,[1] L. Wang,[1] L. Jiu,[1] J. Bruckbauer,[2] Y. Gong,[1] Y. Zhang,[1] J. Bai,[1] R. W. Martin,[2] and T. Wang[1,a)]
[1]*Department of Electronic and Electrical Engineering, University of Sheffield, Mappin Street, Sheffield S1 3JD, United Kingdom*
[2]*Department of Physics, SUPA, University of Strathclyde, Glasgow G4 0NG, United Kingdom*

(Received 12 November 2016; accepted 12 February 2017; published online 27 February 2017)

Exciton localization generally disturbs uniform population inversion, leading to an increase in the threshold current for lasing. High Al content AlGaN is required for the fabrication of deep ultra-violet (DUV) laser diodes (LDs), and this also generates exciton localization. Temperature-dependent photoluminescence and room temperature cathodoluminescence measurements have been performed on high quality semi-polar (11-22) $Al_xGa_{1-x}N$ alloys with high Al composition ranging from 0.37 to 0.56 in order to systematically study the optical properties (in particular, exciton localization) of both the near-band-edge emission and the basal-plane stacking faults related emission, demonstrating different behaviours. Further comparison with the exciton localization of their *c-plane* counterparts has been performed, exhibiting that the exciton localization in semi-polar (11-22) AlGaN is much smaller than that in *c-plane* AlGaN. As a consequence, semi-polar (11-22) AlGaN demonstrates a greater potential than its *c-plane* counterpart in terms of the growth of DUV LDs. [http://dx.doi.org/10.1063/1.4977428]

AlGaN-based deep ultra-violet (DUV) emitters have attracted much attention due to their wide applications in water purification, environmental protection, medical instrumentation, non-line-of-sight communications, etc.[1] The UV emitters reported so far are almost exclusively grown on *c-plane* substrates. This polar orientation leads to built-in electric fields across the active region and thus a reduced quantum efficiency. Another issue is due to exciton localization induced as a result of alloy compositional fluctuations.[2] This issue becomes more severe for the growth of DUV emitters with a sub-280 nm wavelength, where higher Al content (>50%) is required leading to significantly enhanced compositional fluctuations.[3,4] It is well-known that exciton localization plays an important role in improving the quantum efficiency for III-nitride light-emitting diodes (LEDs), in particular, InGaN LEDs,[5] but it disturbs a uniform population inversion, thus leading to an increase in threshold current for lasing.[2] Finally, it is understood that it is another great challenge to achieve a high Al-content p-type AlGaN with good conductivity as a result of its large activation energy. Consequently, the shortest wavelength of the UV laser diodes (LDs) reported so far is limited to 336 nm and such UV LDs can only be operated in pulsed mode with very high thresholds.[6,7]

Building on the experience from InGaN based semi-polar emitters in the visible spectral region,[8] one promising approach forward is to grow UV emitters along semi-/non-polar orientations, which can reduce or eliminate the polarization induced electrical fields. It has also been understood that there exists a significant difference in exciton localization between semi-polar and *c-plane* InGaN. Higher homogeneity of indium composition has been achieved in semi-polar InGaN.[9] Note, however, that atom probe tomography has been used to indicate a greater non-randomness in indium distribution in non-polar InGaN compared to polar *c-plane*.[10] So far, there is no report on the study of the exciton localization in semi-polar AlGaN. Furthermore, it has been predicted theoretically that a higher optical gain could be obtained in semi-/non-polar AlGaN based LDs.[11,12] All these imply that semi-/non-polar AlGaN can possibly exhibit advantages over than its *c-plane* counterpart in terms of growing LDs.

However, owing to great challenges in obtaining semi-/non-polar AlGaN with high quality, there are only a few reports on the studies of the optical properties of such materials. So far, there has been a near complete absence of research on semi-polar AlGaN with high Al composition. Unlike *c-plane* AlGaN, semi-/non-polar AlGaN generally suffers from basal-plane stacking faults (BSFs) in addition to dislocations, further complicating the study of the optical properties of semi-/non-polar AlGaN. Huang *et al.*[13] studied the exciton localization of the BSFs-related emission in non-polar AlGaN with Al composition ranging from 0 to 0.28. Netzel *et al.*[14] investigated the optical polarization properties of both the near-band-edge (NBE) emission and the BSFs-related emission in semi-polar AlGaN. However, in both cases, the BSFs-related emission is hardly distinguished from the NBE emission, thus leading to great challenges in performing detailed studies due to the difficulty in obtaining high-quality AlGaN.

Our group has developed an overgrowth approach of semi-polar (11–22) GaN on micro-rod arrayed templates,[15]

a)Author to whom correspondence should be addressed. Electronic mail: t.wang@sheffield.ac.uk

leading to significantly improved crystal quality of semi-polar (11–22) GaN on sapphire.[16] As a result, high performance semi-polar LEDs with long emission wavelengths out to the amber spectral region have been achieved.[17] Based on this approach, we have further developed a two-step overgrowth approach for (11–22) semi-polar AlGaN exhibiting the best crystal quality compared with other reports. So far, we have achieved a thick and crack-free semi-polar (11–22) AlGaN with Al composition of up to 56%.

In this paper, the optical properties of these high crystal quality (11–22) semi-polar AlGaN samples have been investigated. Both the NBE and the BSFs-related emissions, which have been clearly distinguished as a result of the high crystal quality, have been systematically studied by means of temperature-dependent photoluminescence (PL) and room temperature cathodoluminescence (CL) measurements. Both measurements have been performed in order to study the exciton localization of the NBE and the BSFs-related emissions. More importantly, a detailed comparison study has been performed on these semi-polar AlGaN samples and their *c-plane* AlGaN counterparts with a similar Al composition. All the semi-polar AlGaN samples show a clear reduction in Al composition fluctuations compared with their *c-plane* counterparts. The results presented demonstrate that semi-polar (11–22) AlGaN may be more favourable for being employed to grow DUV LDs than *c-plane* AlGaN.

The semi-polar (11–22) AlGaN samples used were grown by using the two-step overgrowth approach, where thick and crack-free semi-polar (11–22) AlGaN has been achieved by overgrowth on the top of nearly-but-not-fully coalesced GaN deliberately grown on the micro-rod arrayed templates which are similar to those used for the overgrowth of our semi-polar (11–22) GaN.[15–17] The Al composition ranges from 0.37 to 0.56 in each sample. The full width at half maximums (FWHMs) of X-ray diffraction (XRD) rocking curves measured along the [1–100]/[11-2-3] directions (XRD measurements along the two directions are typically used to evaluate the crystal quality of III-nitrides[8]) are 0.2923°/0.2006° for $x = 0.37$ and 0.3825°/0.2064° for $x = 0.56$, respectively, representing the best quality for semi-polar (11–22) AlGaN with a similar Al composition ever reported. It has also been demonstrated that our overgrowth technique can effectively both manage strain and improve the crystal quality simultaneously.

PL measurements were performed by using a doubled-frequency Argon ion laser with an excitation wavelength of 244 nm. For temperature-dependent PL measurements, the samples were held in a helium closed-circuit cryostat with temperature ranging from 10 to 300 K. The luminescence was dispersed using a 0.5 m monochromator and detected using a thermoelectrically (TE) cooled charge-coupled detector (CCD). CL measurements were carried out at room temperature using a field-emission gun scanning electron microscope equipped with a 0.125 m spectrometer and electron multiplying CCD detector and using a Cassegrain reflecting objective to collect luminescence down to 200 nm.[18]

Fig. 1(a) shows the normalized PL spectra measured at 10 K, exhibiting two main peaks in all the samples. Being similar to semi-polar GaN, these two peaks are due to the NBE and BSFs-related emission, respectively. In all PL spectra, a cascade of phonon replica on the low energy side

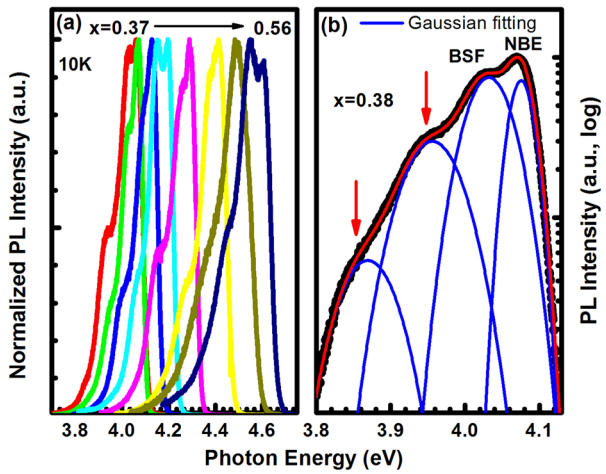

FIG. 1. (a) PL spectra of our semi-polar (11-22) $Al_xGa_{1-x}N$ measured at 10 K; (b) PL spectrum for the $Al_xGa_{1-x}N$ with $x = 0.38$. The red arrows show LO phonon replicas, and the blue lines are the Gaussian fitting curves.

of the main peaks has also been observed, with an energy spacing of around 95–100 meV as shown in Fig. 1(b), where the PL spectrum of the $Al_xGa_{1-x}N$ sample with $x = 0.38$ is provided in a logarithmic scale as an example. The LO phonon energy obtained for our AlGaN samples agrees well with the LO phonon energy reported for GaN (91 meV)[19] and AlN (110 meV).[20]

Although the NBE and the BSF emissions are clearly separated at a low temperature, a fitting using multiple Gaussian curves has been made in order to obtain the accurate emission peak energies of these two emissions. Fig. 1(b) presents an example about our fitting.

Fig. 2(a) shows the emission energies and their separation of the NBE and the BSFs-related emission as a function of Al composition, exhibiting that the BSFs-related emission is about 41 meV and 52 meV lower than that of the NBE emission when the Al composition is 0.37 and 0.56, respectively. Furthermore, Fig. 2(a) demonstrates that the emission energy separation between the NBE and the BSFs-related

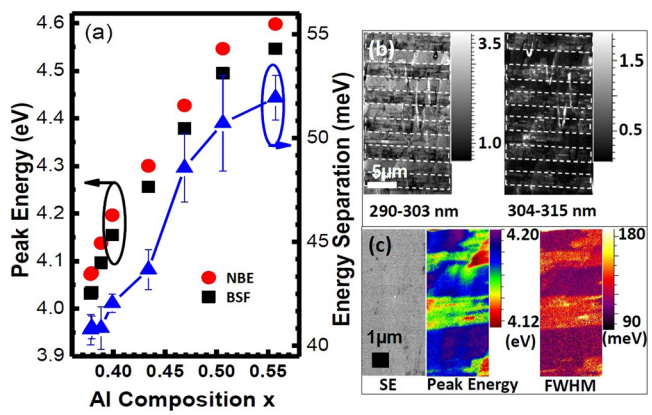

FIG. 2. (a) Emission peak energies of the NBE (labelled as red circles) and the BSFs-related emissions (labelled as black squares), and their energy separation (labeled as blue triangles) as a function of Al composition; (b) integrated CL intensity images with a detected wavelength at 290–303 nm (left) and 304–315 nm (right), respectively, where the dashed rectangles indicate BSFs regions; and (c) high spatial resolution CL imaging in a chevron-free region: Secondary electron image (left), emission peak energy image (middle), and emission peak FWHM image (right).

emissions increases with increasing Al composition, agreeing with the other report.[13]

Generally speaking, the emission energy separation between NBE and BSFs-related emission is also affected by the difference of their respective exciton binding energies and their localization energy difference. Tischer *et al.*[21] reported that the energy separation between the NBE and the BSFs-related emission in semi-polar AlGaN is larger than that in GaN, suggesting that the BSFs regions exhibiting a cubic core with lower Al composition serving as a "quantum well" (QW) are sandwiched by the regions without containing BSFs as "barriers." Assuming that the composition discrepancy between such "QWs" and such "barriers" increases with increasing Al composition, the exciton binding energy difference between NBE and BSFs-related emission will be enhanced with increasing Al composition. Another possible reason for the increase of the energy separation involves the polarization field induced quantum-confined Stark effect (QCSE) in BSF regions. Lahnemann *et al.*[22] suggested that the spontaneous polarization at the wurtzite/zinc-blende interface could result in electric fields across the BSFs regions, leading to a redshift of the BSF related emission. The spontaneous polarization induced electrical fields are expected to be stronger with increasing Al composition.[23] Moreover, there also exists strain-induced QCSE, which will be enhanced as a result of increasing Al composition, further enhancing the energy spacing with increasing Al composition.

To further characterize the emission properties of AlGaN alloys, room temperature CL measurements were carried out on the $Al_xGa_{1-x}N$ sample with $x = 0.40$ as an example. The excitation voltage used is 5 kV, corresponding to an electron penetration depth of ~100 nm, and thus only the emission from the AlGaN can be detected. Since BSFs are two dimensional extended defects embedded in a basal plane, they appear as sets of parallel lines or bundles in CL or transmission electron microscope (TEM) images.[16,24] The room temperature CL shows two dominant emissions in the region 290–315 nm, which we attribute to NBE emission from regions of different composition. As shown by the CL intensity variations in Fig. 2(b), BSFs-related regions (dashed rectangles) are separated by BSF-free regions, forming a periodic distribution on the AlGaN surface. Such a distribution is similar to that observed in the TEM images of our overgrown GaN,[16] suggesting that the BSFs within the underlying GaN extend to the top AlGaN layer. The majority of the surface is dominated by the NBE emission at about 297 nm, as observed in the CL intensity image with an integration window of 290–303 nm (left side of Fig. 2(b)). The CL intensity image integrated over 304–315 nm reveals a different Al content at the chevrons (running perpendicular to the stripes), where the NBE peak is shifted to approximately 305 nm as shown in the right side of Fig. 2(b)).

High spatial resolution CL was performed to further investigate the emission characteristics of the NBE in a chevron-free region. Fig. 2(c) shows the CL peak energy and the FWHM images of the sample, alongside the corresponding secondary electron (SE) image of the mapped area. The area where BSFs are present exhibits a lower emission energy at ~4.14 eV and a broader CL linewidth (FWHM) of ~150 meV, compared to the area where there are no BSFs (with an emission energy of ~4.18 eV and a CL linewidth of ~100 meV). The broader linewidth is most likely due to the lower quality of the material in that region with a high density of BSFs, which also leads to the apparent shift in energy.

In order to investigate the exciton localization arising from the Al compositional fluctuations in $Al_xGa_{1-x}N$ alloys, temperature-dependent PL measurements have been performed. In all cases, the peak energy of the NBE exhibits the same "S" shape behavior when the temperature increases from 10 to 300 K, namely, it redshifts initially, then blueshifts, and finally redshifts. Such a behavior has been widely reported in the *c-plane* $Al_xGa_{1-x}N$ as an indicator of the existence of localized states.[4] The initial redshift is due to carrier redistribution to deeper localized states via a hopping process. With increasing temperature, the carriers are delocalized to higher energy states, giving rise to a blueshift in peak energy. The redshift at higher temperatures is due to the temperature induced bandgap shrinkage. Being similar to the *c-plane* $Al_xGa_{1-x}N$, such "S" shape behavior for the NBE in semi-polar AlGaN is also to be attributed to the Al compositional fluctuation induced exciton localization. In contrast, the temperature dependent behavior of the BSFs-related emission shows a different story. For the samples with a low Al composition ($x < 0.43$), the emission peak still exhibits the similar "S" shape behavior as the NBE does, whereas the samples with a high Al composition ($x > 0.43$) show a redshift and then a blue shift only. The typical temperature-dependent PL spectra corresponding to the above two regions are shown in Figs. 3(a) and 3(b), where the samples with 0.40 Al content and 0.56 Al content are used as examples, respectively. As shown in Fig. 3(b), the BSFs-related emission quenches quickly at high temperatures. With a higher Al incorporation, higher density of defects, e.g., partial dislocations associated with the BSFs and the threading dislocations, are expected. They act as non-radiative recombination centers, contributing to the fast thermal quench at high temperatures observed in the samples with a higher Al-content.

Fig. 4 shows the temperature dependence of the emission peak energies of the NBE and the BSFs-related emissions. The modified Varshni equation based on a band-tail-filling

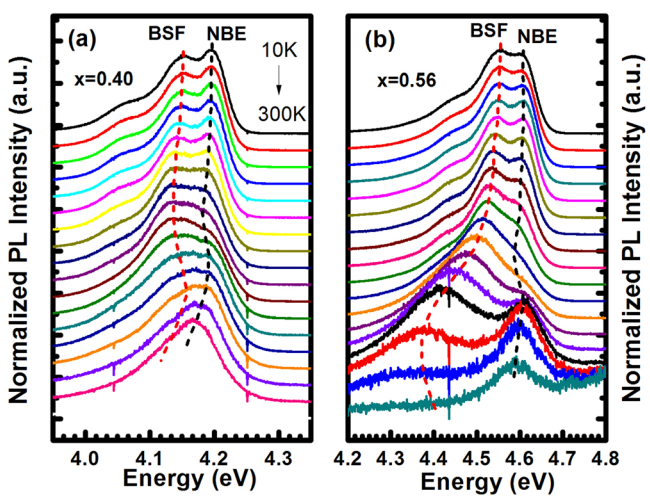

FIG. 3. Temperature-dependent PL spectra of the semi-polar (11-22) $Al_xGa_{1-x}N$ with (a) $x = 0.40$; and (b) $x = 0.56$. The dash lines show the emission energy shift of the NBE and BSFs.

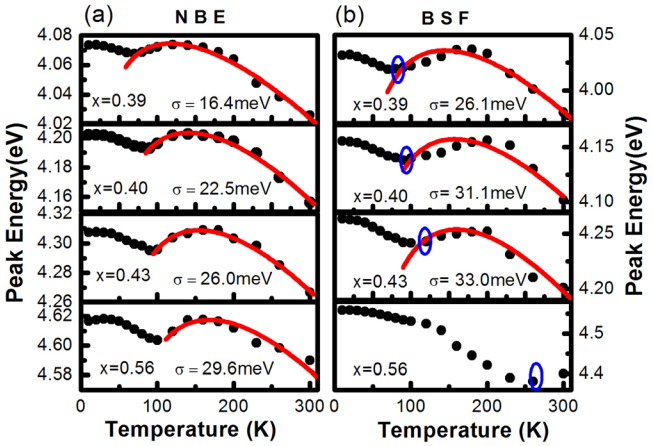

FIG. 4. Peak energy shifts for (a) the NBE and (b) BSFs-related emissions of the semi-polar (11-22) $Al_xGa_{1-x}N$ with $x = 0.38$, 0.40, 0.43, and 0.56. The red solid lines represent the fitted curves by using the modified Varshni equation in order to obtain the exciton localization depth. The blue circles in (b) indicate the transition temperatures.

model, $E(T) = E(0) - \alpha T^2/(T+\beta) - \sigma^2/k_BT$, has been widely used in InGaN and can be employed to fit the emission peak energy, where $E(0)$ is the band gap energy of $Al_xGa_{1-x}N$, α and β are the fitting parameters, k_B is the Boltzmann's constant, and σ is the localization depth which represents an estimated degree of localization. The best fitting in both the NBE and the BSFs-related emissions can be obtained with $\alpha = (1\text{–}1.18) \times 10^{-3}$ eV/K and $\beta = (1100\text{–}1500)$ K, which are comparable with the values reported for their *c-plane* counterparts.[25] For $Al_xGa_{1-x}N$ with $0.45 < x < 0.56$, it is difficult to estimate the localization depth of the BSFs-related emission as a result of the quenching of BSFs-related emission at high temperatures. However, it could be estimated from a transition temperature at which the emission peak energy switches from a redshift to a blueshift. When the Al composition increases from 0.39 to 0.43, the localization depth increases from 26 to 33 meV, where the corresponding transition temperature increases from 80 to 100 K. Given that the transition temperature is as high as 230 K for the sample with 56% Al content, the localization depth of the BSFs-related emission should be much higher than 33 meV.

The obtained localization depths of the NBE and the BSFs-related emission have been provided in Fig. 4. When the Al composition increases from 0.37 to 0.56, the localization depth of the NBE increases from 16 to 29 meV, while the localization depth of the BSF related emission increases from 26 to 33 meV with increasing Al content from 0.38 to 0.43, about 10 meV larger than that of the NBE. One possible reason is due to the Al redistribution in BSF regions as mentioned above.[21] Such a compositional discrepancy between the BSF regions (serving as "QWs") and the BSF-free regions (serving as "barriers") forms a kind of "hereto-structure," roughening their interface sharpness. Being similar to InGaN/GaN systems, this kind of interfacial roughness enhances the exciton localization. Furthermore, the localization effect in BSFs can be further enhanced as a result of the generation of the donor nuclei in the vicinity of BSFs. As Corfdir *et al.*[26] highlighted, the coupling between donor nuclei and BSFs could lead to the localization of electrons within the plane of BSFs in a-plane GaN. In our $Al_xGa_{1-x}N$, in particular, the high Al contained AlGaN, the generation of these extrinsic donors is probably further enhanced, as a large ratio of Al precursor/Ga precursor is required.

TABLE I. Localization depths of semi-polar (11-22) AlGaN and *c-plane* AlGaN.

	Semi-polar (11-22) AlGaN		*c-plane* AlGaN[27]	
x	σ(NBE) (meV)	PL FWHM (meV)	σ(NBE) (meV)	PL FWHM (meV)
0.38	16.4	31	50	40
0.40	22.5	35	51.7	41.8
0.43	26.0	39	54.2	43.1
0.56	29.6	48	69	52

It is interesting to compare the exciton localization in semi-polar (11–22) AlGaN with that in c-plane AlGaN.[4,27,28] The typical values of the localization depths and the low temperature PL line-width in *c-plane* $Al_xGa_{1-x}N$ with various Al composition, which are extracted from Ref. 27, have been summarized in Table I. It can be observed that the localization depth of the NBE increases from 50 to 69 meV when the Al composition increases from 0.37 to 0.56 in *c-plane* AlGaN, which are considerably larger than those of the semi-polar (11–22) AlGaN with a similar Al composition. It means that the exciton localization in semi-polar (11–22) AlGaN is generally weaker than that in its *c-plane* counterpart. This is further confirmed by the PL linewidths, where the PL emission of the semi-polar (11–22) AlGaN is generally narrower than that of its counterpart. As mentioned above, a reduced localization depth leads to an increase in optical gain and thus a reduction in threshold for lasing. This means that semi-polar (11–22) AlGaN exhibits major advantages over than its c-plane counterpart, in particular, in the growth of DUV LDs. Of course, a further improvement in crystal quality is necessary, as BSFs and their associated partial dislocations in semi-polar AlGaN can also affect the performance of LDs such as threshold for lasing.

We have investigated the optical properties of a number of semi-polar (11–22) $Al_xGa_{1-x}N$ samples with Al composition ranging from 0.37 to 0.56. A combination of temperature-dependent PL and room temperature CL measurements, have been performed in order to study both NBE and BSFs-related emissions. The energy separation between the two emissions increases with increasing Al composition, which is mainly ascribed to the compositional discrepancy within BSF regions and enhanced QCSE also within the BSF regions. A detailed study of exciton localization of the NBE and the BSFs-related emissions has been performed, showing that the localization depth of the BSFs-related emission is larger than that of the NBE in each sample. Most importantly, the localization depth of semi-polar (11–22) AlGaN is generally smaller than that of its *c-plane* counterpart, suggesting that semi-polar (11–22) AlGaN is more favourable for the growth of DUV LDs than its counterpart. Our results provide a deep insight into the optical properties of semi-polar AlGaN, which is of significant importance to the development of semi-polar AlGaN based DUV LDs.

Financial support is acknowledged from the Engineering and Physical Sciences Research Council (EPSRC), UK via Grant No. EP/M003132/1. The data associated with this research are available with the corresponding author (dx.doi.org/10.15129/4e3bf564-a341-44b6-993d-8bc3274d9875).

[1]G. Tamulaitis, Lith. J. Phys. **51**, 177 (2011).
[2]M. Adachi, Jpn. J. Appl. Phys. **53**, 100207 (2014).
[3]K. Wang, K. P. O'Donnell, B. Hourahine, R. W. Martin, I. M. Watson, K. Lorenz, and E. Alves, Phys. Rev. B **80**, 125206 (2009).
[4]K. B. Lee, P. J. Parbrook, T. Wang, F. Ranalli, T. Martin, R. S. Balmer, and D. J. Wallis, J. Appl. Phys. **101**, 053513 (2007).
[5]Y. Narukawa, Y. Kawakami, S. Fujita, and S. Nakamura, Phys. Rev. B **59**, 10283 (1999).
[6]H. Yoshida, Y. Yamashita, M. Kuwabara, and H. Kan, Appl. Phys. Lett. **93**, 241106 (2008).
[7]H. Yoshida, Y. Yamashita, M. Kuwabara, and H. Kan, Nat. Photonics **2**, 551 (2008).
[8]T. Wang, Semicond. Sci. Technol. **31**, 093003 (2016).
[9]M. Funato, A. Kaneta, Y. Kawakami, Y. Enya, K. Nishizuka, M. Ueno, and T. Nakamura, Appl. Phys. Express **3**, 021002 (2010).
[10]F. Tang, T. Zhu, F. Oehler, W. Y. Fu, J. T. Griffiths, F. C.-P. Massabuau, M. J. Kappers, T. L. Martin, P. A. J. Bagot, M. P. Moody, and R. A. Oliver, Appl. Phys. Lett. **106**, 072104 (2015).
[11]A. A. Yamaguchi, Appl. Phys. Lett. **96**, 151911 (2010).
[12]K. Kojima, A. A. Yamaguchi, M. Funato, Y. Kawakami, and S. Noda, J. Appl. Phys. **110**, 043115 (2011).
[13]H.-M. Huang, Y.-C. Wu, and T.-C. Lu, J. Electrochem. Soc. **158**, H491 (2011).
[14]C. Netzel, J. Stellmach, M. Feneberg, M. Frentrup, M. Winkler, F. Mehnke, T. Wernicke, R. Goldhahn, M. Kneissl, and M. Weyers, App. Phys. Lett. **104**, 051906 (2014).
[15]Y. Gong, K. Xing, B. Xu, X. Yu, Z. Li, J. Bai, and T. Wang, ECS Trans. **66**, 151 (2015).
[16]Y. Zhang, J. Bai, Y. Hou, R. M. Smith, X. Yu, Y. Gong, and T. Wang, AIP Adv. **6**, 025201 (2016).
[17]J. Bai, B. Xu, F. G. Guzman, K. Xing, Y. Gong, Y. Hou, and T. Wang, Appl. Phys. Lett. **107**, 261103 (2015).
[18]P. R. Edwards, L. K. Jagadamma, J. Bruckbauer, C. Liu, P. Shields, D. Allsopp, T. Wang, and R. W. Martin, Microsc. Microanal. **18**, 1212 (2012).
[19]V. Y. Davydov, Y. E. Kitaev, I. N. Goncharuk, A. N. Smirnov, J. Graul, O. Semchinova, D. Uffmann, M. B. Smirnov, A. P. Mirgorodsky, and R. A. Evarestov, Phys. Rev. B **58**, 12899 (1998).
[20]T. Onuma, S. F. Chichibu, T. Sota, K. Asai, S. Sumiya, T. Shibata, and M. Tanaka, Appl. Phys. Lett. **81**, 652 (2002).
[21]I. Tischer, M. Frey, M. Hocker, L. Jerg, M. Madel, B. Neuschl, K. Thonke, R. A. R. Leute, F. Scholz, H. Groiss, E. Müller, and D. Gerthsen, Phys. Status Solidi B **251**, 2321 (2014).
[22]J. Lahnemann, U. Jahn, O. Brandt, T. Flissikowski, P. Dogan, and H. T. Grahn, J. Phys. D: Appl. Phys. **47**, 423001 (2014).
[23]E. T. Yu, X. Z. Dang, P. M. Asbeck, S. S. Lau, and G. J. Sullivan, J. Vac. Sci. Technol. B **17**, 1742 (1999).
[24]R. Liu, A. Bell, F. A. Ponce, C. Q. Chen, J. W. Yang, and M. A. Khan, Appl. Phys. Lett. **86**, 021908 (2005).
[25]R. Passler, J. Appl. Phys. **90**, 3956 (2001).
[26]P. Corfdir, J. Ristic, P. Lefebvre, T. Zhu, D. Martin, A. Dussaigne, J. D. Ganiere, N. Grandjean, and B. Deveaud-Pledran, Appl. Phys. Lett. **94**, 201115 (2009).
[27]N. Nepal, J. Li, M. L. Nakarmi, J. Y. Lin, and H. X. Jiang, Appl. Phys. Lett. **88**, 062103 (2006).
[28]G. Steude, B. K. Meyer, A. Goldner, A. Hoffmann, F. Bertram, J. Christen, H. Amano, and I. Akasaki, Appl. Phys. Lett. **74**, 2456 (1999).